Super-Resolution in Position and Velocity Estimation for Short-Range MM-Wave Radar

A. Gupta(1), U. Madhow(1) and A. Arbabian(2)

(1) ECE Department, University of California, Santa Barbara, CA, USA
(2) EE Department, Stanford University, Stanford, CA, USA
Emails: {anantgupta, madhow}@ece.ucsb.edu, {arbabian}@stanford.edu

***Abstract*—Recently developed super-resolution algorithms have demonstrated performance approaching fundamental estimation-theoretic bounds. These algorithms have significant potential for applications such as vehicular situational awareness using low-cost, short-range millimeter wave radar sensors. In this paper, we show that such algorithms can approach single-sensor estimation-theoretic bounds for range and Doppler estimation. We also investigate, under a simple 2D model, the limits of position and radial velocity estimation performance of one shot estimation and provide insights for array design.**

I. Introduction

While radar-based target localization (i.e., estimation and tracking of position and velocity) is a classical problem with a rich history, it remains an area of active investigation, including recent work on high-resolution joint estimation of range and Doppler [1], as well as multi-target tracking [2]. In this paper, we investigate the design of millimeter (mm) wave radar system design for short- to medium-range settings, targeting applications such as vehicular situational awareness, with the goal of tracking targets such as pedestrians and bicycles. Accurate estimation and tracking of azimuthal angles for targets is important for such applications, which requires measurements over a large baseline. Fortunately, given advances in low-cost silicon implementation and packaging for mm-wave transceivers, it becomes feasible to deploy a moderately large array of sensors for this purpose. Our goal in this paper is to explore the design of such low-cost sensor arrays, taking advantage of recent advances in super-resolution algorithms [3].

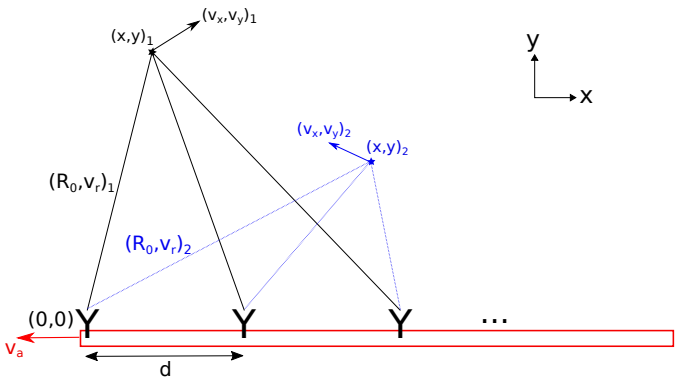

Fig. 1: An array of monostatic sensors.

As depicted in Figure 1, we consider an array of omni-directional monostatic radars spaced by $d \gg \lambda$ (where λ is the carrier wavelength), placed along the X-axis along which the array moves. For distant objects where target range is significantly larger than array inter element distance, a Fourier Transform along the array dimension can be used to extract azimuth angle. However, for the shorter ranges (comparable to inter-sensor distance) of interest to us, fewer sensors spaced appropriately can be sufficient to estimate the position. Since precise carrier frequency/phase synchronization across sensors separated by 10s-100s of wavelengths is difficult, we assume that that the sensors are monostatic. That is, each sensor receives a backscattered version of its own transmitted signal.

While the concepts developed here are quite general, for concreteness, we consider Frequency Modulated Continuous Wave (FMCW) chirp waveforms, which are the most widely used modulation scheme for car radars because of the simplicity of hardware and signal processing relative to, say, pulsed radar, which requires separate delay and frequency estimation for range and Doppler, respectively. The FMCW beat signal contains both range and Doppler information embedded in the frequency domain, and is traditionally extracted using an efficiently implementable 2D Discrete Fourier Transform (DFT), with the "fast time" dimension along a chirp, and the "slow time" dimension across several chirps. However, this technique is susceptible to "off-grid" effects[4]: the signal from a target leaks into several points in the DFT grid, unless it lies exactly on a DFT grid point. While the location estimate can be refined by using a larger number of chirp sequences and sensors, accurate one-shot estimation is especially important for automotive applications, given the importance of timely estimates (which limits the number of frames) and cost/form factor constraints (which limits the number of sensors) [5].

Contributions and Organization: In Section II, we model a single sensor, and show, via estimation-theoretic bounds, that a typical link budget for a low-cost sensor suffices to provide accurate range-Doppler estimates. In Section III, we discuss how measurements from multiple sensors are combined. Estimation algorithms, based on adaptation of recently developed super-resolution algorithms [3], [6], [7], are discussed in Section IV. Section V contains numerical results illustrating the effect of array geometry and the efficacy of the proposed algorithms. Section VI contains our conclusions.

II. Per-Sensor Modeling and Design

A. Signal model

Each radar sensor transmits a Linear Frequency Modulated continuous wave (LFMCW) frame containing N_{ch} chirps which sweep bandwidth B over chirp ramp duration T_m. The transmitted signals across sensors are assumed to be orthogonal to others for any delay or Doppler shift, hence we can model the signals for each sensor separately [8]. We skip many details due to space restrictions, highlighting only the essential modeling steps.

The transmitted signal from any given sensor is a constant envelope signal with complex envelope $e^{j\phi(t)}$, ignoring scaling. The phase increment relative to the carrier is given by $\phi(t) = \int 2\pi f(t)dt$, where $f(t) = s(t \bmod T_m)$, with $s = \frac{B}{T_m}$ denoting the chirp slope (we ignore reset time between chirps). Thus, for the n^{th} chirp, we have $f(t) = st_n$, writing $t = t_n + nT_m$ for the n^{th} chirp, with t_n denoting "fast time" within the chirp, and n indexing "slow time" across chirps.

The downconverted received signal from K targets is given by

$$s_r(t) = \sum_{k=1}^{K} \alpha_k e^{j\phi(t-\tau_k)} e^{-2\pi f_c \tau_k} + w(t) \qquad \tau_k = \frac{2R_k(t)}{c}$$

where α_k is the complex amplitude of the reflected signal (depends on reflectivity and range [9]), $R_k(t)$ is instantaneous range of k^{th} target, and $w(t)$ is white complex gaussian noise.

Deramping against the original chirp waveform, we obtain the beat signal

$$b(t) = s_r(t)e^{-j\phi(t)} = \sum_{k=1}^{K} \alpha_k e^{j2\pi(-f_c\tau_k + st_n\tau_k - \frac{s\tau_k^2}{2})} + w(t) \tag{1}$$

Sampling at rate $1/T_s$, we obtain, after some simplifications and approximations, the discrete-time signal

$$b_{m,n} = \sum_{k=1}^{K} \alpha_k e^{j\left(\underbrace{mT_s\left(Qv_r^k + PR_o^k\right)}_{\text{Fast time}} + \underbrace{Qv_r^k nT_m}_{\text{Slow time}}\right)} + w_{m,n} \tag{2}$$

where $P = \frac{4\pi s}{c}$, $Q = \frac{4\pi f_c}{c}$, $m \in \left[-\frac{N_i}{2}, \frac{N_i}{2} - 1\right]$ is fast time index, $N_i = \frac{T_m}{T_s}$, $n \in \left[-\frac{N_{ch}}{2}, \frac{N_{ch}}{2} - 1\right]$ is slow time index. (Constant phases are absorbed into the $\{\alpha_k\}$).

We can now rewrite in a form that clearly brings out the roles of fast and slow time:

$$b_{m,n} = \sum_{k=1}^{K} \alpha_k e^{j\left(m\omega^f T_s + n\omega^s T_m\right)} + w_{m,n}$$

where $\omega^f = Qv_r^k + PR_o^k$, $\omega^s = Qv_r^k$.

We can consolidate the samples into an observed signal matrix B:

$$B = A + W \tag{3}$$

$$A = \sum_{k=1}^{K} \alpha_k \begin{bmatrix} 1 & e^{j\omega_k^f T_s} & e^{j2\omega_k^f T_s} & \cdots \\ e^{j\omega_k^s T_m} & e^{j\left(\omega_k^f T_s + \omega_k^s T_m\right)} & \cdots & \vdots \\ e^{j2\omega_k^s T_m} & \vdots & \ddots & \vdots \\ \vdots & \cdots & \cdots & \ddots \end{bmatrix}$$

Standard range-Doppler estimation amounts to extracting the frequencies ω^f across rows (fast time) and ω^s across columns (slow time), typically using a 2D DFT. This is susceptible to "off-grid" effects and inter-target interference. Before discussing algorithms that address these problems, we establish limits on the achievable performance via link budgets and estimation-theoretic bounds.

B. Link budget

Our link budget calculations use studies on Radar Cross section of human targets [10], and typical low-cost 60 GHz CMOS transceiver specifications. The signal to noise ratio (SNR) for FMCW radar is calculated by [11]:

$$SNR = \frac{P_{CW} G_t G_r \lambda^2 \sigma_{RCS}}{(4\pi)^3 R^4 L k T F_R B_{IF}}$$

where P_{CW} is the average transmitted power, kTF_RB_{IF} is the receiver noise power, G_t, G_r are antenna gains, R is target range, L is system loss, σ_{RCS} is the radar cross-section (RCS), and B_{IF} is the IF Bandwidth.

Considering 0 dBm transmitted power per sensor (which is easily generated at 60 GHz, for example, by CMOS power amplifiers), $B_{IF} = 1$ MHz and short ranges ($R \sim 10$ m), the operating signal to noise ratio (SNR) is above -10 dB. We now use estimation-theoretic bounds to establish that we can indeed hope to obtain satisfactory performance in this regime.

C. Single-sensor performance limits

Cramer-Rao Bound (CRB): The CRB provides a lower bound on the sample covariance of range-Doppler estimates, $Cov(r, v_r) \geq FIM(r, v_r)^{-1}$. CRB is computed as inverse Fisher Information Matrix (FIM), i.e. $Cov(r, v_r) \geq FIM(r, v_r)^{-1}$. We obtain

$$FIM(r, v_r) = \sum_{m,n} \frac{2|\alpha_i^2|}{\sigma^2} \begin{bmatrix} Pt_n \\ Qt \end{bmatrix} \begin{bmatrix} Pt_n & Qt \end{bmatrix}^*$$

where $|\alpha_i^2|$ is signal power received at i^{th}sensor, $t = mT_s + nT_m$, $t_n = mT_s$.

The result is analogous to the well known result for range-Doppler FIM in, for example ([12], 10.2).

Ziv-Zakai Bound (ZZB): CRB describes behavior of likelihood function around the true value of parameter being estimated. However, at low SNR, it is possible to make large errors in parameter estimation which are not captured by the CRB. The ZZB captures the effect of large errors at low SNR via a hypothesis testing framework, while behaving like the CRB at high SNRs. Since the quantity to be estimated is periodic in nature, we use the vector periodic bound (VPB) result from [13]. We omit details due to lack of space.

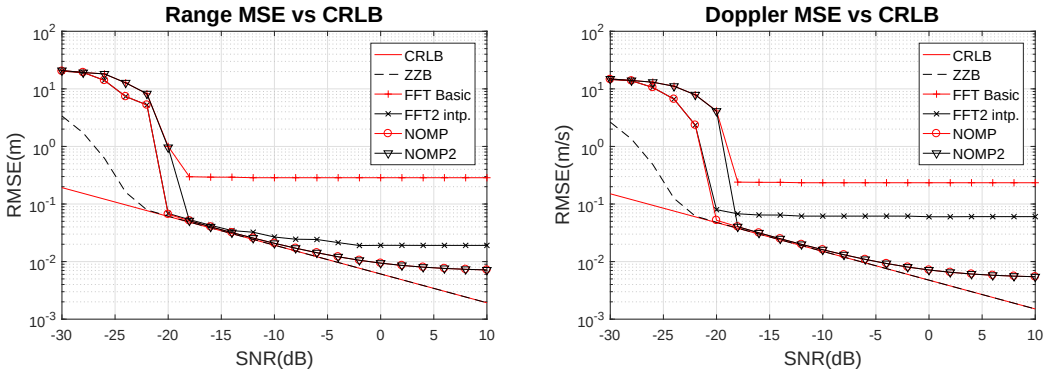

Fig. 2: Per-Sensor range-Doppler estimation performance limits.

The ZZB and CRLB for range estimation are computed numerically and plotted in Figure 2. We conclude from the figure that the ZZB threshold, at which point the ZZB converges to the CRLB, is approximately -22 dB. A sensible choice, therefore, is to design our monostatic sensor such that we operate comfortably beyond the ZZB threshold for delay estimation at the maximum range of interest, given a typical radar cross-section of interest. The example link budget in Section II-B satisfies this.

III. Multi-sensor system

We consider a linear radar array is placed on the side of car moving along the x-axis with velocity v_a. The observed scene can be modeled in two dimensional space with radar 1 at origin and other radars placed in a linear array d meter apart along the x-axis. The system objective is to locate K targets in the scene with inital coordinates $[x_o, y_o]^k$ moving at constant velocity $[v_x, v_y]^k$.

Assuming target radial velocity remain relatively unchanged during a frame, the instantaneous target range at sensor i,

$$R_i^k(t) = R_{oi}^k + v_{ri}^k t \tag{4}$$

$$R_i^k(t) = R_{oi}^k + v_{ri}^k(t_n + nT_m) \tag{5}$$

where $R_{oi}^k = \sqrt{x_i^2 + y^2}$ is range at chirp index 0, $x_i = x + id; y$ are initial coordinates, $v_{ri}^k = (v_x + v_a)\frac{x_i}{R_{oi}^k} + v_y\frac{y}{R_{oi}^k}$ is radial velocity.

From our per-sensor model, we can readily observe that signal frequency along chirp ('fast-time') depends on both range & radial velocity while frequency across chirps ('slow-time') depends only on radial velocity.

A. Performance limits

The Fisher information matrix for estimating the target parameters $\theta = (x, y, v_x, v_y)$ is given by

$$FIM(\theta) = \sum_{i=1}^{N_t}\sum_{m,n}\frac{2|\alpha_i^2|}{\sigma^2}\boldsymbol{\mu}\boldsymbol{\mu}^H$$

where, $\boldsymbol{\mu} = \left[\frac{Pt_n x_i}{R_{oi}} \quad \frac{Pt_n y_i}{R_{oi}} \quad Qt\frac{x_i}{R_{oi}} \quad Qt\frac{y}{R_{oi}}\right]^T$

The upper and lower block diagonal of inverse FIM matrix provides the covariance of position and velocity respectively. Note that for $N_t = 1$, the FIM is singular, which is consistent with the fact that a single sensor cannot provide cross-range resolution for positioning.

IV. Estimation Algorithms

We first discuss algorithms for range-Doppler extraction at each sensor, and then discuss fusion across sensors.

A. Per-Sensor Super-Resolution

2D-FFT: The simplest and most widely used method for extracting frequencies of the rows and columns is to perform 2-D Fourier transform on matrix B. Ideally, all targets should appear as distinct peaks with magnitude proportional to α_k on top of a constant noise floor in the 2-D spectrum. However, as mentioned before, this approach suffers from "off-grid" effects and inter-target interference.

Improved algorithms: Traditional frequency estimation methods such as **MUSIC** give superior performance at the cost of higher computations. A recent frequency estimation method, called Newtonized Orthogonal Matching Pursuit (NOMP), combines greedy pursuit with refinements using Newton's method [3], outperforms classical MUSIC. This algorithm has been generalized to 2D for spatial frequency estimation for 2D arrays [7]. In this paper, we consider this generalization, as well as a simplification thereof, for range-Doppler estimation with multiple targets. We show that these super-resolution algorithms are far superior to the FFT, and approach estimation-theoretic bounds.

2D NOMP: The 2D-NOMP algorithm in [7] can be applied to extract frequencies (ω^f, ω^s) such that,

$$\omega^f, \omega^s = arg\min_{\omega^f,\omega^s}\left\|\mathbf{b\text{-}a}(\omega^f, \omega^s)\right\|^2$$

where $\mathbf{b} = \mathbf{a} + \mathbf{w}$ is the vectorized form of Eq. 3. An initial coarse estimate is obtained using Interpolated 2D FFT followed by Newton refinement steps to get the final estimate.

NOMP2: The cost function to be minimized in each greedy step of 2D-NOMP can be expressed as

$$S_{2D}(g, \omega^f, \omega^s) = \left\|B_{res} - g\mathbf{u}(\omega^f)\mathbf{v}^H(\omega^s)\right\|_F^2$$

$$g, \omega^f, \omega^s = arg\max_{g,\omega^f,\omega^s}\Re(g^H\mathbf{u}^H B_{res}\mathbf{v}) - \frac{1}{2}g^H g\mathbf{u}^H\mathbf{u}\mathbf{v}^H\mathbf{v}$$

Instead of using a 2D-FFT to get an initial estimate for (ω^f, ω^s) as in 2D-NOMP, we reduce complexity in NOMP2 by employing a rank 1 SVD followed by two 1-D FFTs. The refinement Newton step remains the same (see [7] for details).

B. Multi-sensor Processing

In order to obtain the 2D position and velocity of targets, an association algorithm is required to process the range, doppler pairs estimated at each sensor. Design and evaluation of association algorithms will be reported in other publications. We assume here an oracle association algorithm. The position and velocity estimates are solutions to the following optimization problem:

$$\min_{x_0,y_0} \sum_{i=1}^{N_t} \left(r_i - \left\| \begin{bmatrix} x_0 \\ y_0 \end{bmatrix} - \begin{bmatrix} x_{sensor} \\ y_{sensor} \end{bmatrix} \right\| \right)^2 \tag{6a}$$

$$\min_{v_x,v_y} \sum_{i=1}^{N_t} \left(r_i + v_i t - \left\| \begin{bmatrix} v_x \\ v_y \end{bmatrix} - \begin{bmatrix} x_0 - x_{sensor} \\ y_0 - y_{sensor} \end{bmatrix} \right\| \right)^2 \tag{6b}$$

V. Numerical Results

The following results compare the estimation accuracy of methods discussed before for range-Doppler estimation. The number of targets is known *a priori* for these results. The system parameters used for our results are as follows: $f_c = 60$ GHz, $B = 150$ MHz, $T_m = 50\mu$s, $N_{ch} = 64$, $d = 1$ m, $f_s = 1.28$ MHz. We assume that the array is stationary (worst-case in terms of effective aperture). The frame duration is $N_{ch}T_m = 3.2$ ms.

The "Rayleigh resolution" limits (which are easily surpassed by super-resolution algorithms) corresponding to these parameters are as follows [11]: range resolution $\Delta R = \frac{c}{2B} = 1$ m and radial velocity resolution $\Delta v_r = \frac{c}{2f_c T_f} = 0.78$ m/s. The maximum unambiguous range $R_{max} = N_i \Delta R = 64$ m and the maximum unambiguous radial velocity $v_{r,max} = \pm\frac{c}{4f_c T_m} = \pm 25$ m/s.

A. Array design

We first illustrate the effect of changing system parameters on position accuracy in a static setting ($v = 0$). A naive way to visualize this is by drawing two arcs at $R \pm 2\sigma$ from each sensor to get the approximate 95% confidence region for the radar array configurations [14]. We utilize the lower bound on 2D position covariance matrix obtained from CRLB calculations in Section III-A to quantify the position estimation accuracy. Assuming the error in (x,y) are jointly normally distributed, the resulting confidence region is approximated as an ellipse centered at the true location. Figure 3 shows the 95% error ellipse is confined within confidence region formed from arcs satisfying intuition.

The coverage area of the sensor array can be defined in terms of error ellipse area, A_E

$$A_E = \pi\sqrt{6|C|} = \pi\sqrt{6|\text{FIM(x,y)}|^{-1}}$$

To illustrate this, we plot coverage region contours (area of uncertainty region less than A_E) for $N_t = 2$ sensors

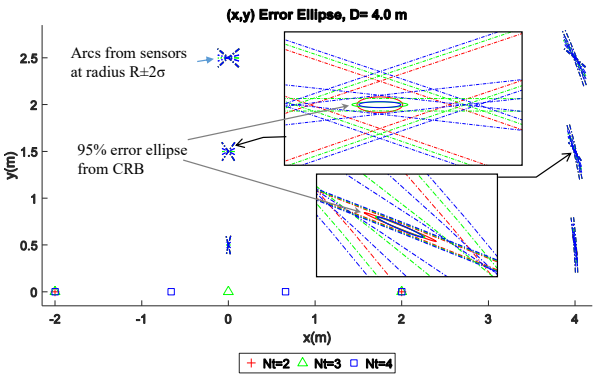

Fig. 3: Confidence region for position estimates.

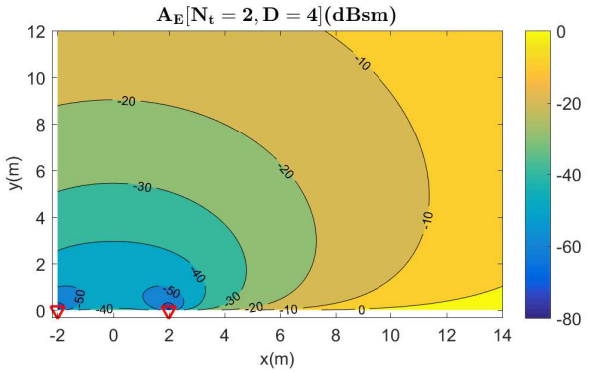

Fig. 4: Coverage areas.

with separation $D = 4$ m in Figure 4. We observe that coverage region does not vary by increasing number of sensors with fixed array length and total radiated power. However, increasing the array length increases maximum coverage range at expense of some degradation in localization accuracy in immediate vicinity. These plots provide insights for sensor placement.

B. Super-Resolution in Range-Doppler

The simulated scene contains 3 targets moving at randomly chosen range and velocity with amplitude adjusted to have equal SNR.

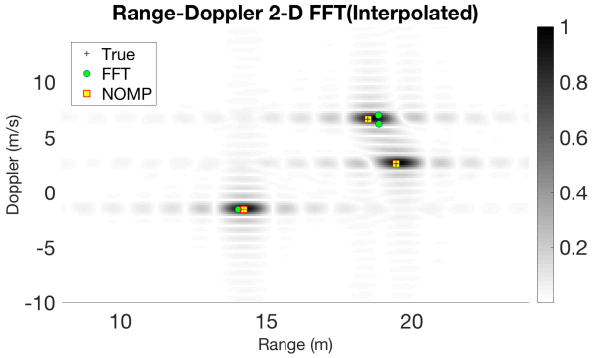

Fig. 5: Range-Doppler response of 3 targets.

2D NOMP and the simplified NOMP2 have similar performance (and are therefore not plotted separately in Figure 5), and are significantly better than conventional methods. The computational cost is compared in Figure 6: we see that NOMP2 is substantially less complex thatn 2D NOMP, while still incurring a higher cost than the standard FFT-based technique.

NOMP based super-resolution algorithms achieves higher accuracy and approaches the CRB in the operating SNR region around -10dB.

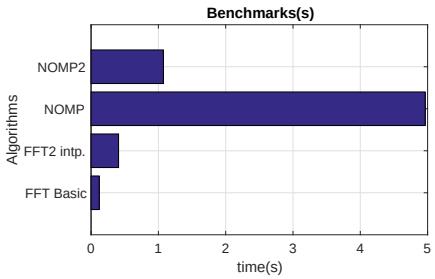

Fig. 6: Comparison of computational cost.

C. Position and Velocity Estimation

Using the range and Doppler estimates from two sensors separated by $d = 2$ m, we estimate the absolute motion parameters, $\theta = \{x, y, v_x, v_y\}$ by solving Eq. 6 using an off-the shelf algorithm. Preliminary results (Fig. 7) show that super-resolution in range-Doppler estimates translate to better position, velocity estimation.

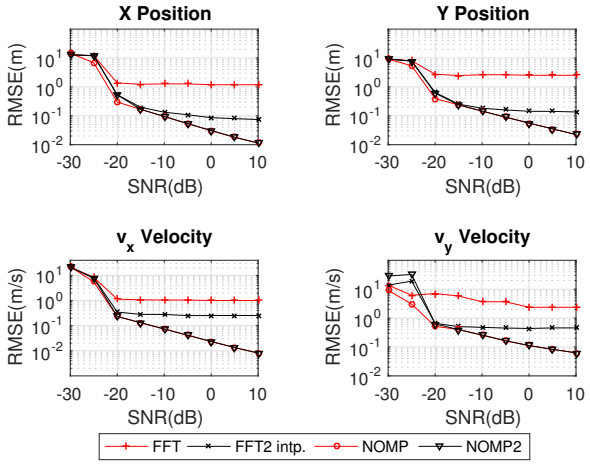

Fig. 7: Position, Velocity Estimation Error.

VI. Conclusion

The estimation-theoretic bounds computed here indicate that it should be possible to get adequate resolution in both position and velocity using a small number of low-cost sensors. Super-resolution algorithms for per-sensor range-Doppler estimation yield performance close to the estimation-theoretic bounds. Combining these measurements over multiple sensors yields accurate position and velocity estimates, as long as the array geometry is suitably designed. These promising results motivate our ongoing work on developing a multi-sensor target tracking framework. While we have considered a simple point target model here, more sophisticated extended target models become important at short ranges [15], [16], and will be incorporated into our future work.

VII. Acknowledgment

This work was supported in part by Systems on Nanoscale Information fabriCs (SONIC), one of the six SRC STARnet Centers, sponsored by MARCO and DARPA, and by the National Science Foundation under Grant No. CNS-1518812, CNS-1518632.

References

[1] B. Demissie and C. R. Berger, "High-resolution range-doppler processing by coherent block-sparse estimation," *IEEE Transactions on Aerospace and Electronic Systems*, vol. 50, no. 2, pp. 843–857, April 2014.

[2] R. Deming, J. Schindler, and L. Perlovsky, "Multi-target/multi-sensor tracking using only range and doppler measurements," *IEEE Transactions on Aerospace and Electronic Systems*, vol. 45, no. 2, pp. 593–611, April 2009.

[3] B. Mamandipoor, D. Ramasamy, and U. Madhow, "Frequency estimation for a mixture of sinusoids: A near-optimal sequential approach," in *2015 IEEE Global Conference on Signal and Information Processing (GlobalSIP)*, Dec 2015, pp. 205–209.

[4] Y. Chi, L. L. Scharf, A. Pezeshki, and A. R. Calderbank, "Sensitivity to basis mismatch in compressed sensing," *IEEE Transactions on Signal Processing*, vol. 59, no. 5, pp. 2182–2195, 2011.

[5] P. Häcker and B. Yang, "Single snapshot doa estimation," *Advances in Radio Science*, vol. 8, pp. 251–256, 2010.

[6] W.-D. Wirth, "Radar techniques using array antennas," 2013.

[7] Z. Marzi, D. Ramasamy, and U. Madhow, "Compressive channel estimation and tracking for large arrays in mm-wave picocells," *IEEE Journal of Selected Topics in Signal Processing*, vol. 10, no. 3, pp. 514–527, April 2016.

[8] M. Steinhauer, H.-O. Ruob, H. Irion, and W. Menzel, "Millimeter-wave-radar sensor based on a transceiver array for automotive applications," *IEEE transactions on microwave theory and techniques*, vol. 56, no. 2, pp. 261–269, 2008.

[9] R. E. Blahut, *Theory of Remote Image Formation*. New York, NY, USA: Cambridge University Press, 2004.

[10] N. Yamada, Y. Tanaka, and K. Nishikawa, "Radar cross section for pedestrian in 76ghz band," in *Microwave Conference, 2005 European*, vol. 2. IEEE, 2005, pp. 4–pp.

[11] M. Jankiraman, N. Willis, and H. Griffiths, *Design of multi-frequency CW radars*. SciTech Pub., 2007.

[12] H. L. Van Trees, *Detection, Estimation, and Modulation Theory Part III*. Wiley, 2001.

[13] S. Basu and Y. Bresler, "A global lower bound on parameter estimation error with periodic distortion functions," *IEEE Transactions on Information Theory*, vol. 46, no. 3, pp. 1145–1150, 2000.

[14] V. Chernyak, "About the use of bistatic measurements for higher object localization accuracy in multisite radar systems," in *2009 International Radar Conference "Surveillance for a Safer World" (RADAR 2009)*, 2009, pp. 1–6.

[15] B. Mamandipoor, G. Malysa, A. Arbabian, U. Madhow, and K. Noujeim, "60 ghz synthetic aperture radar for short-range imaging: Theory and experiments," in *2014 48th Asilomar Conference on Signals, Systems and Computers*, Nov 2014, pp. 553–558.

[16] B. Mamandipoor, M. Fallahpour, G. Malysa, K. Noujeim, A. Arbabian, and U. Madhow, "Spatial-domain technique to overcome grating lobes in sparse monostatic mm-wave imaging systems," in *2015 IEEE MTT-S International Microwave Symposium, San Francisco, CA*, May 2016.